Simulation of vacancies in a two-dimensional Ising antiferromagnet

W. Bauer and S. E. Koonin
W. K. Kellogg Radiation Laboratory 106-38, California Institute of Technology, Pasadena, California 91125
(Received 28 March 1988)

We present simulations of one- and two-vacancy states in a two-dimensional square-lattice Ising antiferromagnet. We find that the energy of the single-vacancy ground state scales as $J^{2/3}$, where J is the spin-spin coupling. The S- and P-wave states of two vacancies are bound, with binding energy $\mathcal{E} \propto J^{2/3}$ and J, respectively, while the D-wave state is unbound.

I. INTRODUCTION

The discovery of copper-oxide-based high-temperature superconductors[1,2] has stimulated a large number of theoretical and experimental investigations[3] and generated interest in non-phonon-mediated pairing. Because of the high transition temperatures and the small isotope effects,[4] it is believed that superconductivity in these new materials arises primarily from strongly interacting electrons, rather than from phonons. In addition, these materials exhibit antiferromagnetic correlations.[5]

There have been suggestions that vacancies in the anti ferromagnetically ordered copper-oxide planes form pairs and thus give rise to superconductivity.[6] A fully microscopic description of this phenomenon could be found, for example, in the Hubbard model near half-filling.[7,8] However, more tractable models of vacancies in spin systems (Heisenberg or Ising) could yield equivalent descriptions with reduced complexity.

There have been several studies along these latter lines. In Ref. 9, a finite basis of states is diagonalized to find one- and two-vacancy states in a square two-dimensional (2D) antiferromagnet. In Ref. 10, the approximation of no closed loops (introduced in Ref. 11 for single vacancy when there is no coupling) was extended to finite couplings for both one- and two-vacancy Ising systems.

In this paper, we employ Monte Carlo methods to study both a single vacancy and the interaction of two vacancies in a 2D square-lattice Ising antiferromagnet. Our method is, in principle, exact and in practice is subject only to statistical and discretization errors, both of which can be controlled. We find binding of two vacancies in states with spatial S and P symmetries.

Our presentation is organized as follows. In Sec. II we introduce the model and describe how our basis states are constructed. In Sec. III the Monte Carlo procedure used to solve the path-integral problem is discussed. Section IV will present the numerical results of our studies for some test cases, for which analytic results are available, and for one and two vacancies in Ising antiferromagnets. A discussion of our results can be found in Sec. V.

II. THE MODEL

We investigate the Ising truncation of the two-dimensional Hubbard Hamiltonian in the large-U limit,

$$\mathcal{H} = -t \sum_{\langle i,l\rangle,\sigma} (c_{i\sigma}^{\dagger} c_{l\sigma} + \text{H.c.}) + J \sum_{\langle i,l\rangle} s_{3i} s_{3l} = \mathcal{H} + \mathcal{V} \; , \tag{1}$$

where the summation extends over all nearest-neighbor pairs of sites $\langle il\rangle$ on a 2D square lattice, and $J = t^2/U$. $c_i^{\dagger}$ and c_i are the usual Fock-space fermion creation and annihilation operators, and the spin operators are defined as $s_{3i} = \sum_{\sigma,\sigma'} c_{i\sigma}^{\dagger} \tau_{\sigma\sigma'}^{3} c_{i\sigma'}$, where τ^3 is the Pauli matrix

$$\begin{bmatrix} 1 & 0 \\ 0 & -1 \end{bmatrix} .$$

In particular, we are interested in the strong-coupling limit ($|J| \ll t$) near half-filling. Depending upon the sign of J, this Hamiltonian describes a ferromagnet ($J<0$) or an antiferromagnet ($J>0$) with holes.

We restrict our Hilbert space to states composed of unoccupied or singly occupied sites; doubly occupied sites are excluded, consistent with large U. A convenient set of basis states is specified by $\{\sigma\}$, the values of the spins at every lattice site, for which we will use the symbols + and − for spin up and down, and 0 for empty sites. As we study here the cases in which there are zero, one, or two vacancies present in an otherwise half-filled lattice, it is convenient to label the basis states by the spatial coordinates of the vacancies. Thus, $|\{\sigma\}\rangle$ represents the case in which no vacancy is present, $|\mathbf{r}_1,\{\sigma\}\rangle$ stands for a one-vacancy state, and $|\mathbf{r}_1\mathbf{r}_2,\{\sigma\}\rangle$ is the symbol for a two-vacancy state.

For convenience, we will set $t=1$ in the following unless it is shown explicitly. Values of the energies, E, and coupling constants, J, given below are then always expressed in units of t.

A. Zero- and one-vacancy states

A zero-vacancy state can be defined as

$$|\{\sigma\}\rangle = \left[\prod_i c_{i\sigma_i}^{\dagger}\right] |0\rangle \; , \tag{2}$$

with 2^{N^2} possibilities for $\{\sigma\}$ on a lattice with N^2 lattice sites. The label i refers to the location of the lattice site, where some standard sequential order of all lattice sites is assumed. The ground state $|\{\sigma\}\rangle$ is ferromagnetic (all spins aligned) for $J<0$ and antiferromagnetic (Néel) for

$J>0$.

We define the one-vacancy states as

$$|\mathbf{r}_1,\{\sigma\}\rangle=(-)^{r_1}c_{r_1\sigma_{r_1}}|\{\sigma\}\rangle$$
$$=(-)^{r_1}c_{r_1\sigma r_1}\left[\prod_i c_{i\sigma_i}^{\dagger}\right]|0\rangle\ , \tag{3}$$

where the state obtained is independent of σ_{r_1}. The phase factor $(-)^{r_1}$ is a "checker-board" phase, which changes sign upon moving to any nearest-neighbor lattice point. The absolute phase is clearly arbitrary, and we choose it so that the phase factor for $\mathbf{r}=(0,0)$ is 1. A general wave function in the space of one vacancy states can then be written as

$$|\Psi_1\rangle=\sum_{\mathbf{r}_1,\{\sigma\}}\Psi(\mathbf{r}_1,\{\sigma\})|\mathbf{r}_1,\{\sigma\}\rangle\ . \tag{4}$$

In the ferromagnetic case, the Hamiltonian is simply diagonalized in the one-vacancy sector. The spins at all sites except the vacancy are aligned ferromagnetically, and the exact energies, relative to the no-vacancy ground state, are

$$e_k=-4J-2(\cos k_x+\cos k_y)\ ,$$
$$k_{x,y}=\frac{2\pi n_{x,y}}{N}\ , \tag{5}$$
$$n_{x,y}=0,\ \pm1,\ \pm2,\ \ldots\pm(N/2-1),\ N/2\ ,$$

where N is the lattice size.

In the antiferromagnetic case, even in the $J\to0$ limit, the one-vacancy states are nontrivial, because a vacancy can scramble the antiferromagnetic spin configuration as it moves through the lattice. Working in the $J\to0$ limit, Brinkman and Rice[11] found that the band is narrowed relative to that given by 5. In an approximation that excludes vacancy paths with closed loops, they find that the band edge is raised from its ferromagnetic value of $E=-4$ to $E=-2\sqrt{3}$ and speculate on the existence of localized states below this energy.

From the anticommutation relations of the operators $c_{i\sigma}$ it is straightforward to derive the following matrix elements:

$$\langle\{\sigma'\}|\{\sigma\}\rangle=\delta_{\sigma\sigma'}\ ,$$
$$\langle\mathbf{r}_1',\{\sigma'\}|\mathbf{r}_1,\{\sigma\}\rangle=\delta_{\sigma\sigma'}\delta_{\mathbf{r}_1\mathbf{r}_1'}\ ,$$
$$\langle\mathbf{r}_1',\{\sigma'\}|\mathcal{V}|\mathbf{r}_1,\{\sigma\}\rangle=V(\sigma)\delta_{\sigma\sigma'}\delta_{\mathbf{r}_1\mathbf{r}_1'}\ , \tag{6}$$
$$\langle\mathbf{r}_1',\{\sigma'\}|\mathcal{H}|\mathbf{r}_1,\{\sigma\}\rangle=-t\delta_{\sigma,\sigma'+\mathbf{n}}\delta_{\mathbf{r}_1,\mathbf{r}_1'+\mathbf{n}}\ ,$$

where $\mathcal{H}$ and $\mathcal{V}$ are the operators defined Eq. (1) and $\mathbf{n}$ is a lattice unit vector. The symbol $\sigma'+\mathbf{n}$ refers to the spin configuration which results by taking the ensemble of spins $\{\sigma'\}$ and exchanging the values of the spins at $\mathbf{r}_1'$ and $\mathbf{r}_1'+\mathbf{n}$ for each other. The δ functions in $\mathbf{r}$ in these equations are already implicitly contained in the δ functions in σ, but we have included them here for clarity of notation. Thus, our basis provides a natural second-quantized language for discussing the one-vacancy sector.

B. Two-vacancy states

A suitable basis for the two-vacancy sector are states of the form

$$|\mathbf{r}_1\mathbf{r}_2,\{\sigma\}\rangle=(-)^{r_1+r_2}c_{r_1\sigma_{r_1}}c_{r_2\sigma_{r_2}}|\{\sigma\}\rangle$$
$$=(-)^{r_1+r_2}c_{r_1\sigma_{r_1}}c_{r_2\sigma_{r_2}}\left[\prod_i c_{i\sigma}^{\dagger}\right]|0\rangle\ , \tag{7}$$

which is antisymmetric under exchange of the two vacancies

$$(|\mathbf{r}_1\mathbf{r}_2,\{\sigma\}\rangle=-|\mathbf{r}_2\mathbf{r}_1,\{\sigma\}\rangle)\ .$$

As in the one-vacancy case, these states are independent of the "dummy" spins at the vacancy sites. A general two-vacancy wave function can be written as

$$|\Psi_2\rangle=\sum_{\mathbf{r}_1\mathbf{r}_2,\{\sigma\}}\Psi(\mathbf{r}_1\mathbf{r}_2,\{\sigma\})|\mathbf{r}_1\mathbf{r}_2,\{\sigma\}\rangle\ , \tag{8}$$

where the antisymmetry of the basis states implies the antisymmetry of the general two-vacancy wave function $|\Psi_2\rangle$.

The matrix elements of operators within these two-vacancy basis states can be calculated in analogy to Eq. (6). However, the fermion nature of the electrons results in additional exchange terms. For example, the scalar product of two basis states is given by

$$\langle\mathbf{r}_1',\mathbf{r}_2'\{\sigma'\}|\mathbf{r}_1\mathbf{r}_2,\{\sigma\}\rangle=\delta_{\sigma\sigma'}(\delta_{\mathbf{r}_1\mathbf{r}_1'}\delta_{\mathbf{r}_2\mathbf{r}_2'}-\delta_{\mathbf{r}_1\mathbf{r}_2'}\delta_{\mathbf{r}_2\mathbf{r}_1'})\ . \tag{9}$$

Thus, our basis states provide a second-quantized language for treating the two-vacancy problem. Their generalization to multivacancy situations is straightforward.

III. MONTE CARLO PROCEDURE

The thermodynamic average of an observable Ω is given in the canonical ensemble by

$$\langle\Omega\rangle=\mathrm{tr}\left[\frac{\Omega e^{-\beta\mathcal{H}}}{\mathrm{tr}(e^{-\beta\mathcal{H}})}\right]\ , \tag{10}$$

where $\mathcal{H}$ is the Hamiltonian of the system as defined in Eq. (1), $\beta=1/kT$ is the inverse temperature, and the trace extends over all states with a given number of vacancies (spin configurations and vacancy locations). However, as we are interested only in the ground states for various numbers of vacancies, we replace the trace in Eq. (10) by an expectation value in a suitable trial state $|\Psi_T\rangle$,

$$\langle\Omega\rangle=\frac{\langle\Psi_T|e^{-\beta\mathcal{H}/2}\Omega e^{-\beta\mathcal{H}/2}|\Psi_T\rangle}{\langle\Psi_T|e^{-\beta\mathcal{H}}|\Psi_T\rangle}\ , \tag{11}$$

in which we specify the initial locations of the vacancies and the spin configuration of the lattice. As β becomes large, $\langle\Omega\rangle$ approaches the ground-state expectation value, as long as $|\Psi_T\rangle$ is not orthogonal to the true ground state. The choice of these trial states in the one- and two-vacancy cases will be discussed below.

A. General method

We evaluate the expectation values in Eq. (11) by discretizing the imaginary time interval $[0,\beta]$ with small slices of width $\Delta\beta$. Upon introducing complete sets of states at each time slice, the sums over intermediate states are carried out via Monte Carlo techniques. We found that a 20×20 lattice with periodic boundary conditions was sufficient for the studies presented here, and that up to 640 time slices were required for adequate accuracy.

To evaluate the propagation of the system over the small time interval $\Delta\beta$, we break up the Hamiltonian into operators whose matrix elements are convenient to evaluate. Such a breakup of $\mathcal{H}$ into plaquettes is well known.[12] We have chosen instead to split the Hamiltonian into

$$\mathcal{H}=(\mathcal{K}_x+\tfrac{1}{2}\mathcal{V})+(\mathcal{K}_y+\tfrac{1}{2}\mathcal{V}) . \tag{12}$$

Since we use basis states in which $\mathcal{V}$ is diagonal, we consider only the kinetic energy operator for the moment and note that

$$e^{-\Delta\beta(\Omega_1+\Omega_2)}=e^{-\Delta\beta\Omega_1}e^{-\Delta\beta\Omega_2}[1+O(\Delta\beta^2)] , \tag{13}$$

which is valid for general operators Ω_1 and Ω_2 with $[\Omega_1,\Omega_2]\neq0$.

If all spins on the lattice were aligned (ferromagnetic configuration), the kinetic energy operators simply would move vacancies around in a straightforward way. Then $\mathcal{K}_x$ and $\mathcal{K}_y$ commute, the factorization of the exponential is exact, and we obtain

$$e^{-\Delta\beta(\mathcal{K}_x+\mathcal{K}_y)}=e^{-\Delta\beta\mathcal{K}_x}e^{-\Delta\beta\mathcal{K}_y} . \tag{14}$$

However, in general (and, in particular, for an antiferromagnetic lattice) the kinetic energy operators must be "protected" by projectors ensuring that no-spin world lines are inadvertently disconnected as a vacancy moves. The general Eq. (13) then applies, and we will have to extrapolate our results to $\Delta\beta=0$.

We now insert $2l-1(l\Delta\beta=\beta)$ complete sets of basis states into the expectation values of Eq. (11) and obtain

$$\langle\Omega\rangle=\frac{\sum_{i_1,\ldots,i_{2l-1}}\langle\Psi_T|e^{-\Delta\beta\mathcal{K}_x}|i_1\rangle\cdots\langle i_l|\Omega e^{-\Delta\beta\mathcal{K}_x}|i_{l+1}\rangle\cdots\langle i_{2l-1}|e^{-\Delta\beta\mathcal{K}_y}|\Psi_T\rangle}{\sum_{i_1,\ldots,i_{2l-1}}\langle\Psi_T|e^{-\Delta\beta\mathcal{K}_x}|i_1\rangle\cdots\langle i_{2l-1}|e^{-\Delta\beta\mathcal{K}_y}|\Psi_T\rangle}$$

$$=\sum_{i_1,\ldots,i_{2l-1}}\frac{\langle i_l|\Omega e^{-\Delta\beta\mathcal{K}_x}|i_{l+1}\rangle}{\langle i_l|e^{-\Delta\beta\mathcal{K}_x}|i_{l+1}\rangle}P(i_1,\ldots,i_{2l-1}) , \tag{15}$$

where $P(i_1,\ldots,i_{2l-1})$ is the probability for the configuration $\{i_1,\ldots,i_{2l-1}\}$,

$$P(i_1,\ldots,i_{2l-1})=\frac{\langle\Psi_T|e^{-\Delta\beta\mathcal{K}_x}|i_1\rangle\cdots\langle i_{2l-1}|e^{-\Delta\beta\mathcal{K}_y}|\Psi_T\rangle}{\sum_{i_1,\ldots,i_{2l-1}}\langle\Psi_T|e^{-\Delta\beta\mathcal{K}_x}|i_1\rangle\cdots\langle i_{2l-1}|e^{-\Delta\beta\mathcal{K}_y}|\Psi_T\rangle} . \tag{16}$$

We sample histories of the system according to this probability distribution in our Monte Carlo procedure.

B. One vacancy

Consider two one-vacancy states $|\mathbf{r}_1,\{\sigma\}\rangle$ and $|\mathbf{r}_1',\{\sigma'\}\rangle$. We will omit reference to the spin configurations from now on, but note that as we need consider, for each time slice, only vacancies moving in one lattice direction, the spin configuration changes in a "natural" way. Then

$$\langle\mathbf{r}'|e^{-\Delta\beta\mathcal{K}_x}|\mathbf{r}\rangle=\delta_{yy'}\langle x'|e^{-\Delta\beta\mathcal{K}_x}|x\rangle . \tag{17}$$

Inserting a complete set of momentum eigenstates of $\mathcal{K}_x$ we obtain

$$\langle x'|e^{-\Delta\beta\mathcal{K}_x}|x\rangle=\sum_{k_x}e^{ik_x(x-x')}e^{\Delta\beta 2t\cos k_x}$$

$$\equiv g(\Delta\beta,x-x') . \tag{18}$$

Consider now the product in the numerator of Eq. (16). In accord with the usual Metropolis sampling strategy, we propose a trial change in the path, say $|\mathbf{r}_i\rangle$, to $|\mathbf{r}_i+\boldsymbol{\mu}\rangle$ where $\boldsymbol{\mu}$ is a lattice unit vector (compare Fig. 1).

$$\langle\mathbf{r}_{i-1}|e^{-\Delta\beta\mathcal{K}_x}|\mathbf{r}_i\rangle\langle\mathbf{r}_i|e^{-\Delta\beta\mathcal{K}_y}|\mathbf{r}_{i+1}\rangle\langle\mathbf{r}_{i+1}|e^{-\Delta\beta\mathcal{K}_x}|\mathbf{r}_{1+2}\rangle$$

$$\rightarrow\langle\mathbf{r}_{i-1}|e^{-\Delta\beta\mathcal{K}_x}|\mathbf{r}_i+\boldsymbol{\mu}\rangle\langle\mathbf{r}_i+\boldsymbol{\mu}|e^{-\Delta\beta\mathcal{K}_y}|\mathbf{r}_{i+1}+\boldsymbol{\mu}\rangle\langle\mathbf{r}_{i+1}+\boldsymbol{\mu}|e^{-\Delta\beta\mathcal{K}_x}|\mathbf{r}_{i+2}\rangle . \tag{19}$$

Upon comparing the first part of this product to Eq. (17), we see that $y_{i-1}=y_i$ and so $\boldsymbol{\mu}=\mu\cdot\hat{\mathbf{x}}$ ($\mu=\pm1$). Because the

second part of the product requires $\delta_{x_i x_{i+1}}$, we have to move $|\mathbf{r}_{i+1}\rangle$ by the same vector $\boldsymbol{\mu}$. We then compute the ratio

$$w=\frac{\langle \mathbf{r}_{i-1}|e^{-\Delta\beta\mathcal{H}_x}|\mathbf{r}_i+\boldsymbol{\mu}\rangle\langle \mathbf{r}_i+\boldsymbol{\mu}|e^{-\Delta\beta\mathcal{H}_y}|\mathbf{r}_{i+1}+\boldsymbol{\mu}\rangle\langle \mathbf{r}_{i+1}+\boldsymbol{\mu}|e^{-\Delta\beta\mathcal{H}_x}|\mathbf{r}_{i+2}\rangle}{\langle \mathbf{r}_{i-1}|e^{-\Delta\beta\mathcal{H}_x}|\mathbf{r}_i\rangle\langle \mathbf{r}_i|e^{-\Delta\beta\mathcal{H}_y}|\mathbf{r}_{i+1}\rangle\langle \mathbf{r}_{i+1}|e^{-\Delta\beta\mathcal{H}_x}|\mathbf{r}_{i+2}\rangle}$$
$$=\frac{g(\Delta\beta,x_i-x_{i-1}+\mu)g(\Delta\beta,x_{i+2}-x_{i+1}+\mu)}{g(\Delta\beta,x_i-x_{i-1})g(\Delta\beta,x_{i+2}-x_{i+1})} . \quad (20)$$

We then use the heat-bath algorithm and accept the proposed configuration with probability

$$p=\frac{w}{1+w} . \quad (21)$$

In the case of a trial state involving vacancies embedded in an antiferromagnetic background, we must exclude vacancy paths that scramble the final spin configuration of the lattice. A simple example of such a forbidden path cited by Brinkman and Rice[11] is when a vacancy travels once around a lattice plaquette. By simply checking that no-spin world lines are disconnected by the trial paths we propose, we can also exclude these paths, as demonstrated in Fig. 2.

Figure 2(a) shows the "once-around-the-plaquette" path must be excluded as it scrambles the spin configuration of the lattice. Indeed, the spin configuration of the lowest time slice differs from that of the highest. In our method of evolving the paths of vacancies the lowest and the highest time slice always retain their spin configurations. In Fig. 2(b) the transition from the first column to the second column represents an allowed move. However, the transition from the second to the third column represents a forbidden move, which is equivalent to the vacancy traveling once around the square plaquette as depicted in Fig. 2(a). Such a forbidden path carries the signature that at least one spin world line is disconnected. This disconnection can be seen in going from the lower right corner of the second time slice from the bottom in column three to the same location in the third time slice from the bottom. Here the spin changes sign from + to −, and we have indicated the disconnected spin world line by a dotted line in Fig. 2.

The inclusion of the potential of Eq. (1) is easy using the breakup of the Hamiltonian given in Eq. (12). Since we work in a basis in which $\mathcal{V}$ is diagonal, we always have

$$\exp\left[-\Delta\beta\frac{\mathcal{V}}{2}\right]|\mathbf{r}\rangle=\exp\left[-\Delta\beta\frac{V(\sigma(\mathbf{r}))}{2}\right]|\mathbf{r}\rangle , \quad (22)$$

where $\exp\{-\Delta\beta[V(\sigma(\mathbf{r}))/2]\}$ is a c number. This implies that Eq. (20) must be modified to

$$w=\frac{g(\Delta\beta,x_i-x_{i-1}+\mu)g(\Delta\beta,x_{i+2}-x_{i+1}+\mu)}{g(\Delta\beta,x_i-x_{i-1})g(\Delta\beta,x_{i+2}-x_{i+1})}$$
$$\times\exp\left[-\frac{\Delta\beta}{2}[V(\sigma(\mathbf{r}_i+\mu))+V(\sigma(\mathbf{r}_{i+1}+\mu))\right.$$
$$\left.-V(\sigma(\mathbf{r}_i))-V(\sigma(\mathbf{r}_{i+1}))]\right] . \quad (23)$$

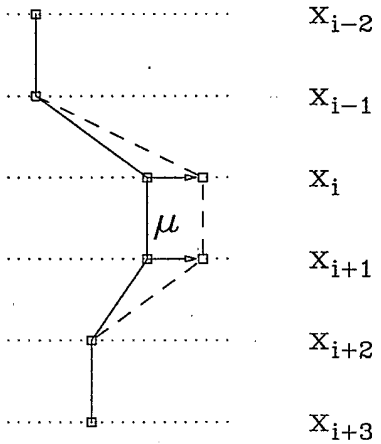

FIG. 1. Illustration of the Monte Carlo method used to solve the path integral problem. The solid line represents a path of a vacancy, where the position of the vacancy at each time slice x_j is given by the squares. Also indicated is a proposed new path resulting from moving the vacancy at time slice x_i by μ (dashed line).

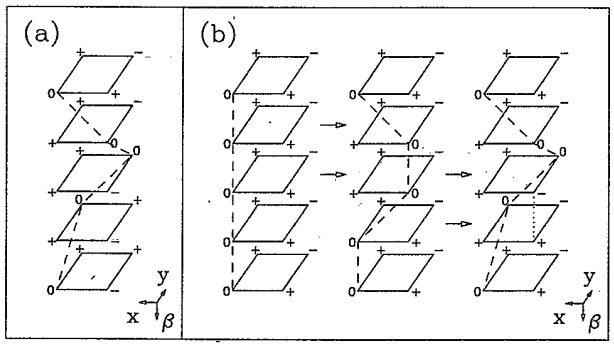

FIG. 2. (a) Example of a forbidden path of a vacancy in the approximation of Brinkman and Rice. The spin configuration of the plaquette in the lowest time slice is scrambled with respect to the highest. (b) The same path (column 3) in our numerical simulation. Here the signature of a forbidden path is the disconnected spin world line between the second and third time slice from the bottom in this column (indicated by the dotted line). The transition from the path of the vacancy in column one to the path in column two is an allowed one, whereas the transition from column two to three is forbidden.

Using the probabilities P from Eq. (16) we can now compute observables. In general this will involve commutators $[\Omega,\exp(-\Delta\beta\mathcal{H})]$ that vanish like $O(\Delta\beta)$ in the case that $[\Omega,\mathcal{H}]$ is nonzero. We will therefore have to extrapolate linearly to $\Delta\beta=0$ for cases where these commutators do not vanish.

The observable of greatest interest is the total energy of the system. This will always involve the computation of the expectation values of the kinetic and the potential energies. The calculation of the potential energy term is simple, since $\mathcal{V}$ is diagonal in our basis. To calculate the kinetic energy, we must evaluate matrix elements like

$$\langle \mathbf{r}_i \mid \mathcal{H}_x e^{-\Delta\beta\mathcal{H}_x} \mid \mathbf{r}_{i+1}\rangle = -t[\langle \mathbf{r}_i+1 \mid e^{-\Delta\beta\mathcal{H}_x} \mid \mathbf{r}_{i+1}\rangle + \langle \mathbf{r}_i-1 \mid e^{-\Delta\beta\mathcal{H}_x} \mid \mathbf{r}_{i+1}\rangle]$$
$$= -t[g(\Delta\beta, x_i - x_{i+1}+1) + g(\Delta\beta, x_i - x_{i+1}-1)]\delta_{y_i y_{i+1}} . \tag{24}$$

C. Two vacancies

Our algorithm for sampling histories of a two-vacancy system is analogous to that we have described for the one-vacancy system. Minor complications arise from the facts that two vacancies cannot be at the same site at the same time and that we have excluded doubly occupied sites from our Hilbert space. The latter results in correction terms to the kinetic energy

$$\langle \mathbf{r}_i \mid \mathcal{H}_x e^{-\Delta\beta\mathcal{H}_x} \mid \mathbf{r}_{i+1}\rangle = -t[\langle \mathbf{r}_i+1 \mid e^{-\Delta\beta\mathcal{H}_x} \mid \mathbf{r}_{i+1}\rangle + \langle \mathbf{r}_i-1 \mid e^{-\Delta\beta\mathcal{H}_x} \mid \mathbf{r}_{i+1}\rangle]$$
$$= -t[g(\Delta\beta, x_i - x_{i+1}+1)(1-\delta_+) + g(\Delta\beta, x_i - x_{i+1}-1)(1-\delta_-)]\delta_{y_i y_{i+1}} , \tag{25}$$

where δ_+ is 1 if there is another vacancy at the lattice site (x_i+1, y_i) and 0 otherwise, and δ_- is 1 if there is another vacancy at the lattice site (x_i-1, y_i) and 0 otherwise. An additional complication is that imposed by the antisymmetry constraint discussed in connection with Eq. (9); we deal with this in the course of discussing our results below.

IV. RESULTS

A. Numerical tests

One simple check of our algorithm is to simulate one vacancy on a ferromagnetic lattice. Here the single-particle energies are given by Eq. (5). The expectation value of the energy is

$$E = \langle \mathcal{H} \rangle = \frac{\sum_k e^{-\beta e_k} e_k}{\sum_k e^{-\beta e_k}}$$
$$= -4J - 2\frac{\sum_k e^{2t\beta\cos k}\cos k}{\sum_k e^{2t\beta\cos k}} . \tag{26}$$

In Fig. 3 we display the exact result of Eq. (26) as a function of β (solid line). The plot symbols represent the result of our Monte Carlo calculations. For every datapoint three runs of the program using 10 000 updates of the path were performed. The results of the Monte Carlo simulation agree completely with the exact calculation within the statistical errors; this is hardly a surprise. Our factorization is exact for all values of $\Delta\beta$ in the case of a ferromagnetic lattice; i.e., Eq. (14) holds. To generate Fig. 3, we have used a constant value of $l=10$ and values of $\Delta\beta$ between 0.025 (corresponding to $\beta=0.25$) and $\Delta\beta=0.8$ (corresponding to $\beta=8$). In all other cases that we consider in this work, Eq. (14) does not hold. We must therefore use small values of $\Delta\beta$ and extrapolate to $\Delta\beta=0$.

We now turn to the case of one vacancy in an antiferromagnetic lattice (our trial state), with $J=0$. As mentioned previously, this problem was addressed by Brinkman and Rice,[11] who found for the two-dimensional square lattice a band edge[13] at $E\approx -2\sqrt{3}$. We have cal-

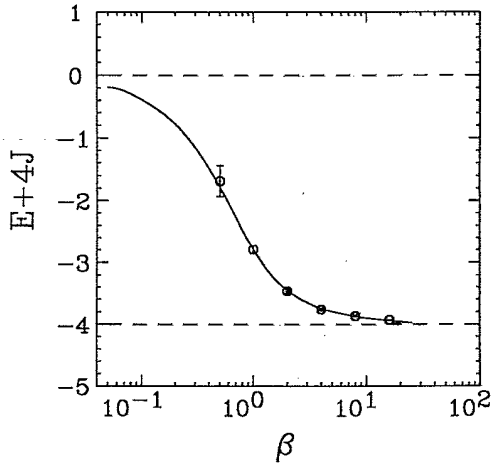

FIG. 3. Energy of the one-vacancy state in a ferromagnetic lattice as a function of β. The solid line represents the exact analytic result, whereas the results of our Monte Carlo calculation are shown by the plot symbols.

culated E for $\beta=8$ and different values of $\Delta\beta$. Since the density of states varies like $\rho(\omega)\propto\sqrt{\omega-\omega_0}$ near the band edge,[11] we would expect a value of

$$E(\beta=8)\approx -2\sqrt{3}+\frac{3}{2\beta}\approx -3.28\ . \tag{27}$$

This value is represented by the dashed line in Fig. 4, while the points are the results of our calculations. For every value of $\Delta\beta$ we performed five independent runs with different seeds of the random number generator and 50 000 updates of each time slice of the path. Our results approach the exact value for $\Delta\beta\to 0$. A linear χ^2 fit and extrapolation to $\Delta\beta=0$ yields the value $E_{\rm calc}(\beta=8)=-3.25\pm 0.07$, accurate within the uncertainty. The addition of more data points with smaller $\Delta\beta$ would not improve the accuracy of the final result since the statistical errors associated with the individual data points increase with decreasing $\Delta\beta$. But even the value for $\Delta\beta=0.1$ is wrong by only 0.1, which will turn out to be acceptable for most applications we deal with in this work. We have therefore used this value of $\Delta\beta$ for the following calculations with $J\neq 0$.

B. One vacancy, $J\neq 0$

Figure 5 shows our results for E as a function of β for different values of J. From top to bottom the J values used are 0.6, 0.2, 0.06, and 0. In all cases the statistical errors are smaller than the plot symbols used. In all four cases calculated the curves approach a constant value for large β. As expected, we find that E increases with increasing J, as it becomes energetically more costly for the vacancy to hop to another site; the vacancy is bound to the origin by a string of overturned bonds.

The functional dependence of E on J is of some interest. Shraiman and Siggia[10] have recently proposed that $E(J')=E(0)+2.74J'^{2/3}$, where their coupling constant, which we call J', is $4J$. We have calculated $E(J)$ at

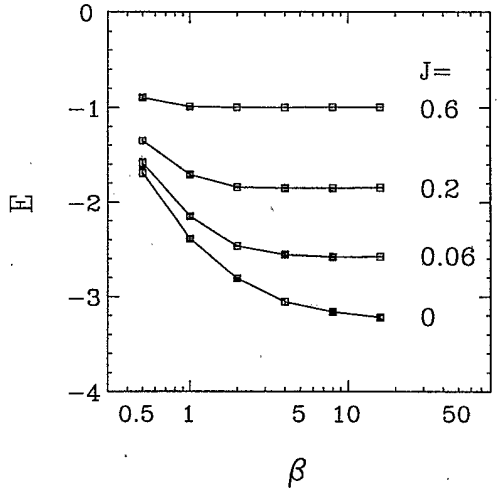

FIG. 5. Energy, E, as a function of β for different values of J in the case of the one-vacancy state.

a finite value of $\beta=8$. The saturation of the curves in Fig. 5 shows that this is a reasonable approximation to $E(J,\beta\to\infty)$. The results of our calculations are displayed in Fig. 6. The data points are represented by the plot symbols, and the solid straight line corresponds to a linear regression fit

$$E(J)-E(0)=aJ^{2/3}+b\ . \tag{28}$$

We extract from our data the values $a=3.15$ and $b=0.06$ with a correlation coefficient $\kappa=0.992$. If this is expressed in terms of J', we obtain a coefficient of $J'^{2/3}$ of 1.25, or less than half of that found by Shraiman and Siggia. We attribute this reduction to self-intersections and juxtapositions of the vacancy path, as already hypothesized in Ref. 10.

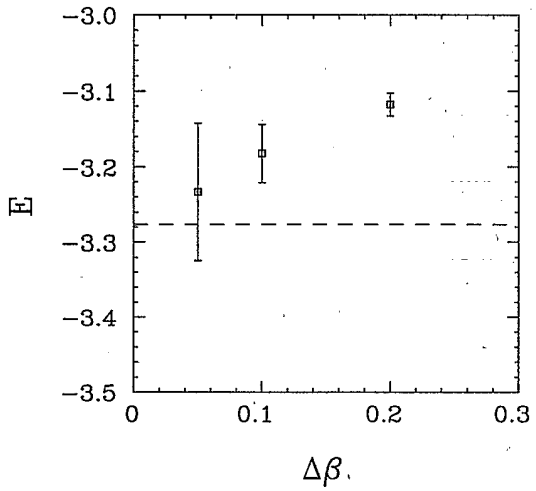

FIG. 4. Numerical test: E as a function of $\Delta\beta$ for the one-vacancy state and $J=0$, calculated at $\beta=8$. The dashed line represents the analytical result of Brinkman and Rice, corrected for the effect of finite temperature.

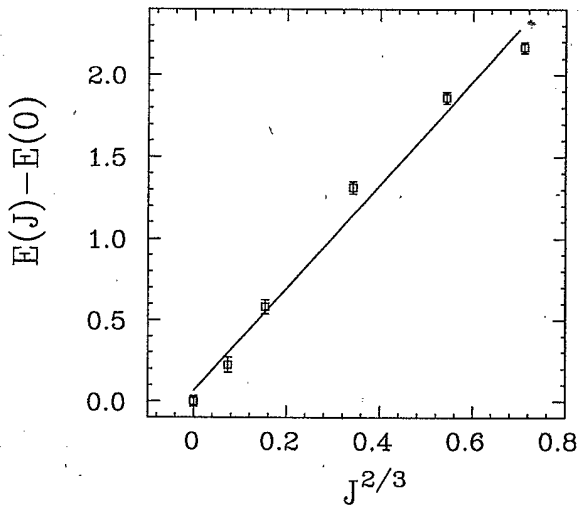

FIG. 6. Energy, E, as a function of $J^{2/3}$ for $\beta=8$ in the one-vacancy case. The squares are the results of our calculations, and the straight line is a linear regression fit $E(J)-E(0)=3.15J^{2/3}+0.06$.

C. Two vacancies

We now turn to the two-vacancy sector for antiferromagnetic couplings. Because of possible connections with the newly discovered high-temperature superconductors, the binding of two vacancies is the most interesting question we can address in this sector. A simple picture[6] leads to the expectation that two vacancies will indeed bind. As one of the vacancies travels through an antiferromagnetic lattice, it leaves behind it a string of energetically unfavorable ferromagnetic bonds, which binds it to the origin. If the second vacancy follows behind the first one, it will "heal" the bonds. The pair would thus be bound together and would not be localized. However, naive expectations that this scenario automatically leads to binding can be countered with a one-dimensional example.[10] It is therefore necessary to perform careful calculations to address this issue.

To investigate the binding of two vacancies, we compare the expectation values of the energy, Eq. (11) with $\Omega=\mathcal{H}$, calculated with different trial states. One of these is our "reference state," consisting of two widely separated vacancies in a Néel background of spins. As long as their separation is large enough and β is finite, it is clear that these two vacancies will never "find each other" to bind, so that the energy found for this state (relative to the no-vacancy Néel state), will simply be twice the energy of a one-vacancy state. We have verified that this is so in our calculations.

The other trial states we use in our calculations have the two vacancies neighboring each other in a Néel background of spins. If one of the vacancies is at the origin [lattice coordinates (0,0)], then the other vacancy is at the neighboring site (1,0) in our "s-wave" trial state (denoted by S), and we impose no restrictions on the paths, other than those described in the previous section. Our first "p-wave" trial state (denoted by P_1) corresponds to this same initial configuration, but we impose the additional requirement that there be a node in the many body wave function [Eq. (8)] along the line $x_1=x_2$. Practically, this is done by simply forbidding Monte Carlo moves that would cause the vacancy paths to have the same x coordinate at any particular time. Our second "p-wave" trial state (P_2) has the second vacancy at the site (1,1), and we impose a nodal surface along the line $x_1-x_2=y_1-y_2$. Finally, our "d-wave" trial state (D) has the same initial configuration of vacancies as P_2, with nodes imposed both along $x_1=x_2$ and along $y_1=y_2$.

In view of the requirement that the two-vacancy wave function be antisymmetric under the interchange of the two vacancies, we regard only the P_1 and P_2 trial states as physical. However, as we do not allow for the most general nodal structure of the wave function, our results for the energies of these state, and for the D state as well, can only be regarded as variational upper bound; i.e., the binding could be greater than what we calculate.

All of our two-vacancy calculations have been performed with $\Delta\beta=0.1$. To check the validity of this approximation, we performed a series of calculations analogous to that used in Fig. 4. For a constant value of $\beta=8$ and a constant value of $J=0.6$ we varied $\Delta\beta$. The upper panel of Fig. 7 shows the results of these tests. The upper curve represents the energy calculated with our reference trial state (R), while the lower curve shows the results obtained with the S trial state. The difference of the two expectation values, which we identify as the binding energy, ε, is displayed in the lower panel of Fig. 7. From these results, it appears reasonable to fix $\Delta\beta=0.1$, since the binding energy we find for this value of $\Delta\beta$ lies com-

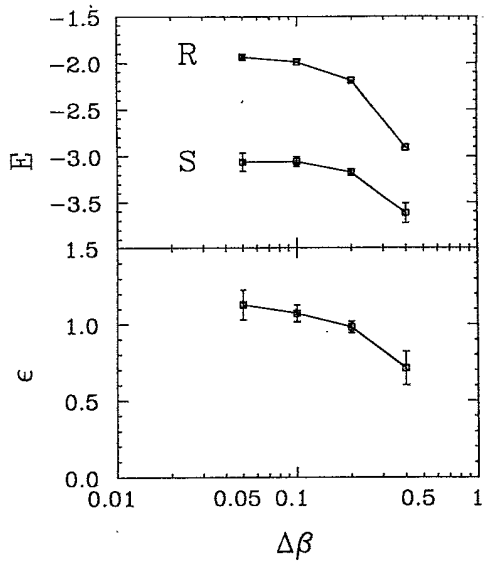

FIG. 7. Numerical test: energy, E, for the states R and S (upper part of figure) and binding energy, ε (lower part), as a function of $\Delta\beta$ for $\beta=8$ and $J=0.6$.

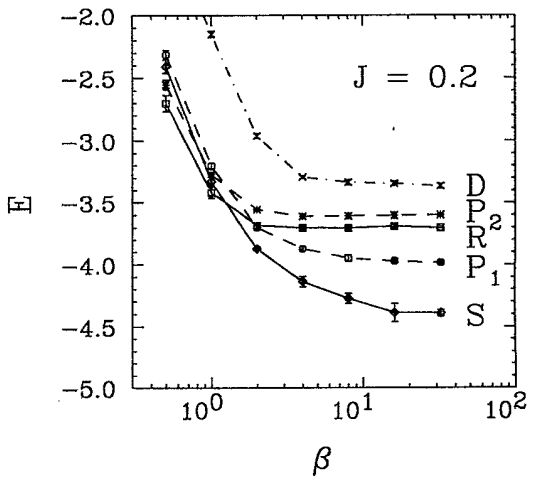

FIG. 8. Energy of the two vacancy states as a function of β for $J=0.2$. The solid line with the square plot symbols (third line from the top at $\beta=32$) corresponds to our reference state of widely separated vacancies (R). The other solid line with the diamond plot symbols (lowest line at $\beta=32$) corresponds to our S trial state Results of calculations with our P_1 state are represented by the dashed line with the octagonal plot symbols (second line from the bottom at $\beta=32$), while those from our P_2 state correspond to the dashed line with the stars (second line from the top at $\beta=32$) and those from our D state are shown by the top line.

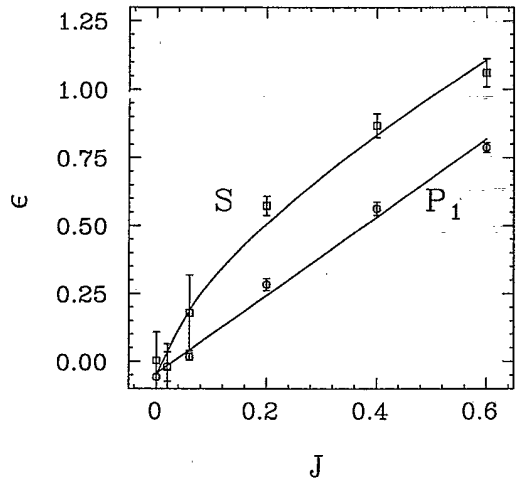

FIG. 9. Binding energy, ε, as a function of J for the S and P_1 symmetry states. The plot symbols represent our calculations, and the straight lines are the results of fits with $\varepsilon \propto J^{2/3}$ and $\varepsilon \propto J$, respectively.

pletely within the uncertainty of our result for $\Delta\beta=0.05$.

In Fig. 8, we present a systematic study of E as a function of β for the different trial states with $\Delta\beta=0.1$. For the smaller values of β, the reference state R has the lowest E; i.e., all of the pair states are unbound. This is because, at low β, the vacancies make few excursions from their trial state locations, so that, for the paired trial states, there is a high probability that they will occupy neighboring lattice sites. In this case, the correction terms to the kinetic energy [Eq. (25)] that arise from excluding two vacancies at the same site become more important.

At the larger values of β, all energies saturate $\beta=8$ and 16. We are therefore confident in drawing conclusions about binding from our finite-β calculations. Both the S and P_1 trial states have asymptotic energies that are lower than that of the reference state; i.e., they are bound. In contrast, the P_2 and D trial states are unbound.

For the bound S and P_1 states we have calculated the binding energy as a function of J. In Fig. 9 we present these binding energies calculated at $\beta=16$, and the plot symbols are the results of our calculation. For the S state, we find binding proportional to $J^{2/3}$, and we extract

$$\varepsilon_S=-0.05+1.63J^{2/3}\ , \tag{29}$$

with a correlation coefficient of $\kappa=0.991$. The P_1 state exhibits binding proportional to J, and we find

$$\varepsilon_{P_1}=-0.05+1.44J\ , \tag{30}$$

with a correlation coefficient of $\kappa=0.996$.

V. DISCUSSION

We have presented Monte Carlo simulations of one and two vacancies in a 2D Ising antiferromagnet. For one vacancy states when $J=0$, we find an energy in agreement with the analytic approximation of Brinkmann and Rice,[11] while for $0<J\lesssim 1$, we find an energy varying as $J^{2/3}$. This latter is in qualitative agreement with the results of Siggia and Shraiman,[10] although our numerical coefficient is less than half of theirs, presumably because of their neglect of self-intersecting and juxtaposed paths.

For two vacancies, we find bound states with both S and P spatial symmetries, but no binding in states with a D symmetry. The binding we find is "strong" for the S state in the sense that the binding energy scales as $J^{2/3}$. For the P spatial symmetry we find binding proportional to J. These results are in qualitative agreement with those of Ref. 10 and in contrast to those of Ref. 9. The former work finds strong binding in S states (although again with a larger numerical coefficient—our S state is to be identified with the boson state of Ref. 10), and weak binding ($\propto J$) in P and D states. The later work finds no binding at all.

As neither of Refs. 10 or 9 is sufficiently detailed for us to make a thorough analysis of their calculations, we can only speculate as to the sources of our discrepancies with them and their discrepancies with each other. The limited basis of Ref. 9 allows the vacancy to be at most three hops away from its initial site, although it does allow the vacancy to travel by translations of the computational unit cell. This implies that the vacancy travels through the lattice with a very localized disturbance of the Néel background. In contrast, our calculations show the vacancy often five or more hops away from its starting site with a substantial scrambling of the Néel background. The method of Ref. 10 allows paths with an arbitrary number of hops, but ignores self-intersections and juxtapositions of the paths, which is probably the reason why these authors obtain numerical coefficients for their binding energies different from ours.

Our calculations presented here can be extended in two interesting ways. One is to consider multi-vacancy states. As the fermion nature of only the vacancies need be treated explicitly, existing Monte Carlo methods tractable for few-fermion systems might be applied; a calculation on a 20×20 lattice with 5% vacancies appears quite feasible.

A second extension is to include spin dynamics. It is likely that the ability of the spins to relax would weaken or destroy the "string" confining a single vacancy and so increase its mobility. The interaction of two vacancies might similarly weaken, although spin fluctuations might also bind two vacancies together.[14] The ideal simulation addressing these ideas would be a spin-$\frac{1}{2}$ Heisenberg system with vacancies. Although the 2D antiferromagnetic Heisenberg model without vacancies can be simulated,[15] we know of no scheme that allows vacancies to be incorporated without encountering the "negative probabilities" that often plague Monte Carlo calculations. However, a tractable alternative is to promote our static Ising spins to the dynamical ones of the $O(3)$ nonlinear σ model. Such a simulation would reveal the influence of spin waves on our present results and also allow study of the importance of topologically nontrivial spin textures and their interaction with vacancies.[16]

ACKNOWLEDGMENTS

The initial phase of this work benefited from S.E.K.'s interactions at the Aspen Center for Physics, with, among others, R. Bhatt, J. Hirsch, A. Ruckenstein, A. P. Young, and M. C. Cross; we thank the latter for his continuing interest in this project at Caltech. This work was supported in part by the National Science Foundation under Grant Nos. PHY86-04197 and PHY85-05682 and by supercomputer time granted by the San Diego Supercomputer Center.

[1]J. G. Bednorz and K. A. Müller, Z. Phys. B **64**, 189 (1986).
[2]P. Chu *et al.*, Phys. Rev. Lett. **58**, 405 (1987).
[3]For references see, *High Temperature Superconductivity* (American Physical Society, New York, 1987).
[4]B. Batlogg *et al.*, Phys. Rev. Lett. **58**, 2333 (1987).
[5]D. Vaknin *et al.*, Phys. Rev. Lett. **58**, 2802 (1987).
[6]J. E. Hirsch, Phys. Rev. Lett. **59**, 923 (1987).
[7]J. Hubbard, Proc. Roy. Soc. (London) A **276**, 283 (1963).
[8]J. E. Hirsch, Phys. Rev. B **31**, 4403 (1985).
[9]S. A. Trugman (unpublished).
[10]B. I. Shraiman and E. D. Siggia, Phys. Rev. Lett. **60**, 740 (1988).
[11]W. F. Brinkman and T. M. Rice, Phys. Rev. B **2**, 1324 (1970).
[12]J. E. Hirsch, R. L. Sugar, D. J. Scalapino, and R. Blankenbecler, Phys. Rev. B **26**, 5033 (1982).
[13]Below the value of E given here, Brinkman and Rice find "localized" states which extend in energy to $E=-4$. However, these states are only accesseble through at least triple loops around a plaquette. For the parameters considered here, we did not find these states in our Monte Carlo samples.
[14]J. R. Schrieffer, X.-G. Wen, and S.-C. Zhang, Phys. Rev. Lett. **60**, 944 (1988).
[15]E. Manousakis and R. Salvador, Phys. Rev. Lett. **60**, 840 (1988).
[16]P. B. Weigmann, Phys. Rev. Lett. **60**, 821 (1988); A. D. Jackson, J. J. M. Verbaarschot, I. Zahed, and L. Castillejo (unpublished); E. D. Siggia and B. I. Shraiman (unpublished).